433

Simulation and modeling of the elliptic streamline flow

By G. A. Blaisdell[1] AND K. Shariff[2]

Direct numerical simulations are performed for the elliptic streamline flow, which is a homogeneous turbulent flow that combines the effects of solid body rotation and strain. Simulations are run over a range of parameters in order to determine the effect of changing rotation and strain separately. For early times the nonlinear cascade is suppressed, but then is re-established at later times. The growth rate of turbulent kinetic energy agrees at early times with the trends from linear theory, but at later times the flow seems to approach an asymptotic state that is independent of the ratio of mean flow rotation rate to strain rate. A comparison with standard Reynolds stress turbulence models is made. It is found that for strong rotation rates, the models predict decay of the turbulence, while the simulations show exponential growth. Close examination of the simulation results shows that they are affected by excessively low Reynolds numbers. Suggestions for reducing low Reynolds number effects in future simulations is given.

---

1. Introduction

1.1 Motivation

The elliptic streamline flow is an important flow for many reasons. This flow contains the effects of both rotation and strain and is therefore similar to the mean flow in a vortex strained in the plane perpendicular to its axis. Such flows provide insight into fundamental vortical interactions within turbulence, and the instability caused by the strain has been proposed as a universal mechanism for energy transfer from large scales to small scales (Pierrehumbert 1986).

A strained vortex also occurs in airplane wakes, in which each wingtip vortex induces a strain field on the other. The strain field can affect the stability of these vortices and thereby their turbulent structure downstream. The ability to understand and predict the turbulent structure of the vortices is important to the wake hazard problem, which is of major concern for the safety of commercial aircraft.

Another example of a flow with the combined effects of rotation and strain is the outer core of the earth's interior. The electrically conducting fluid in the outer portion of the earth's core rotates with the earth but is also strained by tidal forces. A large scale secondary flow results, which has been proposed as the cause of the

1 Purdue University

2 NASA Ames Research Center

magnetic field (Malkus & Berry 1988). Additional examples are flow in fluid-filled satellites and in rectangular cavities.

The elliptic streamline flow is also a good test case for turbulence models for rotating flows. It has an added complication beyond that of pure rotation, but it is still a basic flow. The additional strain rate is present in most practical engineering flows and, therefore, is a necessary effect for turbulence models to capture. As shown in Section 3, standard Reynolds stress models predict decay of the turbulent kinetic energy for cases with strong rotation, whereas the DNS shows exponential growth. Therefore, the elliptic streamline flow presents a challenging case for turbulence modelers.

1.2 Background

The elliptic streamline flow has been studied using Rapid Distortion Theory (RDT) by Cambon *et al.* (1985) and Cambon *et al.* (1994). Different approaches were used by Pierrehumbert (1986), Bayly (1986), and Waleffe (1990), who performed inviscid stability analyses. For circular streamlines (pure rotation) there are no unstable modes, while for elliptic streamlines a band of unstable modes exists in which the growth rate depends on the polar angle of the wavenumber vector. The band of unstable angles increases in width for increasing ellipticity of the streamlines. Also, the growth rate of the unstable modes is independent of the magnitude of the wavenumber vector. Therefore, arbitrarily small three-dimensional fluctuations can be created by an instability of a basic two-dimensional flow. Pierrehumbert suggested that this might be a mechanism for the cascade process in turbulent flows.

The effects of viscosity were studied by Landman & Saffman (1987) and are included in the RDT analyses of Cambon *et al.* The growth rate of the instabilities is modified by viscosity so that the growth rate is no longer independent of the magnitude of the wavenumber vector. Landman & Saffman found a high wavenumber cut-off of the instability. However, there is no low wavenumber cut-off, and arbitrarily large scales are unstable. This fact causes the turbulent eddies to eventually outgrow the computational domain in the DNS discussed below.

An interesting experiment corresponding to elliptic streamline flow was done by Malkus (1989). A tank with moving flexible walls was used to create a flow with elliptic streamlines. He observed a collapse phenomenon in which the two-dimensional flow suddenly breaks down into three-dimensional small scale motions. Waleffe (1990) studied the stability of the enclosed elliptic flow and suggested the collapse phenomenon is due to nonlinear interactions in which the mean flow is altered. It is not clear at this point how this confined flow is related to the homogeneous turbulent flow studied here.

Lundgren & Mansour (1996) investigated the stability of a vortex in a rectangular domain. This flow is very similar to the elliptic streamline flow and displays a similar instability. However, their flow has a mean velocity which decays in time, and their flow is inhomogeneous. These two factors introduce additional complicating effects and make gathering turbulence statistics difficult because of the low statistical sample that is available. The elliptic streamline flow and its instability is also related to the instability of a strained, finite-sized vortex with uniform vorticity

studied by Widnall *et al.* (1974) and others.

An experiment which was designed to correspond to the homogeneous elliptic streamline flow was performed by Benoit (1992). He investigated grid generated turbulence created by a rotating grid and then passed through a specially designed diffuser with elliptic cross-sections. Benoit also analyzed the flow using linear rapid distortion theory. In order to compare with his results, simulations at Reynolds numbers higher than those in the current study are needed. This point is discussed futher below.

There has been a considerable amount of work done on the stability of the elliptic streamline flow. However, the only numerical simulations that have been done are the preliminary simulations of Blaisdell & Shariff (1994). The current simulations are a continuation of that work. With the use of direct numerical simulation, the nonlinear development of the flow and the fully turbulent state can be examined.

1.3 Objectives

The objectives of this work are to investigate the elliptic streamline flow for the fully turbulent case and to provide statistics for comparison with turbulence models. One of the issues to be investigated is whether the linear instability modes grow to dominate the flow even in the presence of large initial disturbances. The effect of the governing parameters on the development of the flow is also to be studied. For the elliptic streamline flow the governing parameters are: (1) the ratio of the rotation rate to the strain rate, which gives the aspect ratio of the elliptic streamlines, (2) the ratio of a mean flow time scale, such as the rotation rate, to the turbulence time scale, and (3) the turbulent Reynolds number. Simulations are chosen to vary these parameters in a systematic way. However, it is found that the Reynolds numbers of these simulations is low enough that the development of the flow is significantly affected. Suggestions for overcoming this limitation in future simulations are discussed in Section 4.

Turbulence statistics, including full Reynolds stress budgets, have been calculated for each of the simulations. One objective was to do a detailed comparison with turbulence models. However, because of the low Reynolds numbers of the current simulations, a meaningful quantitative comparison cannot be done. Nonetheless a brief comparison of the turbulent kinetic energy growth is presented in Section 3.

2. Governing equations & numerical method

Consider homogeneous turbulence with the mean flow

$$U_i = U_{i,j} x_j, \quad U_{i,j} \equiv \begin{pmatrix} 0 & 0 & -\gamma - e \\ 0 & 0 & 0 \\ \gamma - e & 0 & 0 \end{pmatrix}, \tag{1}$$

which describes a one-parameter family of streamline patterns in the x-z plane (the other parameter sets the strength of the flow). The case $\gamma = 0$ corresponds to pure strain with two principal directions at $\pm 45°$ relative to the x-axis while $0 < |\gamma| < |e|$ gives vortical strain dominated flows with hyperbolic streamlines, their asymptotes

being shallower or steeper than the pure strain case according as $(e - \gamma)/(e + \gamma) < 1$ or > 1. The limit $|e| = |\gamma|$ is pure shear. The case $e = 0$ corresponds to pure rotation while $0 < |e| < |\gamma|$ gives vortical rotation dominated flows with geometrically similar elliptic streamlines with aspect ratio $E \equiv \sqrt{(\gamma + e)/(\gamma - e)}$. This case is depicted in Fig. 1.

The code shear_i, developed by Dr. R. S. Rogallo (of Los Altos Hills, Calif.) to run on the Intel parallel computers at NASA Ames for the case of pure shear and employing a subset of the techniques described in Rogallo (1981), was modified to treat the above cases and to run on the IBM SP2 using MPI for message passing. The xz plane was chosen as the plane of deformation to minimize disruption to the code. The program uses the second-order Runge-Kutta scheme to time-advance the Fourier transformed Navier-Stokes equation (notation will be explained momentarily):

$$\frac{d}{dt}(F\widehat{u}_i) = F\left\{\Pi^{(2)}_{ij} U_{j,m}\widehat{u}_m - i\Pi^{(1)}_{ij} k_m \widehat{u_j u_m}\right\} \tag{2}$$

Due to the use of coordinates that deform with the mean flow, the k_i in Eq. (2) represent time-dependent physical wavenumbers:

$$k_i = k'_j B_{ji}(t), \quad \dot{B}_{ij} = -B_{ik}U_{k,j}, \tag{3}$$

while hats denote the three-dimensional Fourier transform with respect to computational wavenumbers k'_i. Space discretization is implied by the restriction of k'_i to integers $-M/2 \leq k'_i \leq M/2$; homogeneity is realized when there is a sufficiently large range of small wavenumbers with energy tending to zero. The symbol $\Pi^{(n)}_{ij} \equiv \delta_{ij} - nk_ik_j/k^2$ with $n = 1$ is the projector applied to the Navier-Stokes equation to eliminate pressure; a slightly different projector, $\Pi^{(2)}_{ij}$, appears in the linear term due to an additional contribution from the time derivative term in deforming coordinates. The aliasing error concomitant with the pseudo-spectral evaluation of $\widehat{u_j u_m}$ is controlled (but not exactly eliminated) by a combination of phase shifting and spherical truncation in which modes with $k'^2 > 2(M/3)^2$ are discarded upon return to wavenumber space. The viscous integrating factor F, satisfying $(1/F)dF/dt = +\nu k^2(t)$, is obtained analytically. Since in the linearized limit exact time integration of (2) is not possible (or at least not trivial, Waleffe 1990), the present version of the program does not treat the rapid distortion limit exactly. Rather, the time step is chosen to be the more restrictive one obtained from the mean flow and the non-linear term. For pure shear the flow-field can be re-meshed to prevent extreme distortion of the computational domain. In the elliptic flow, however, a fluid element undergoes time-periodic shearing and straining, and rather than tackle the corresponding re-meshing problem, small enough ellipticities are considered so that the minimum interior angle of the element, $\theta_{\min} = \tan^{-1}\left[2E/(E^2 - 1)\right]$, does not become too small (for the largest case of $E = 3$ considered, $\theta_{\min} = 37°$).

In Blaisdell & Shariff (1994) the code was tested for: (i) The linear inviscid and viscous behavior of a single Fourier mode compared with the results of Landman &
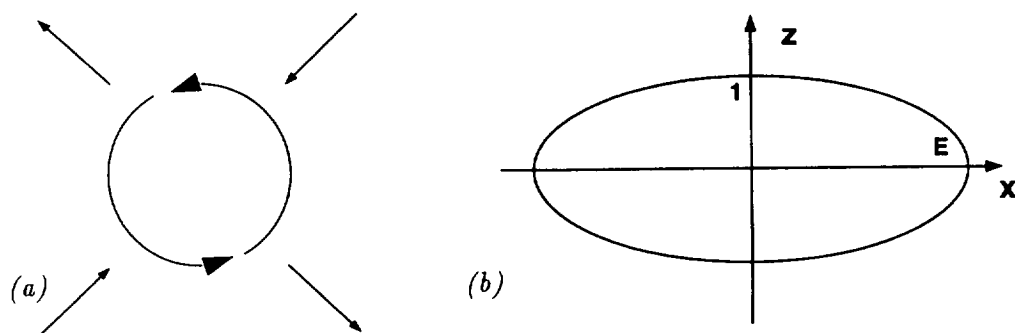
FIGURE 1. *(a)* Schematic view of combination of rotation and strain. *(b)* Elliptic streamline. (The direction of the arrows corresponds to $\gamma > 0$ and $e > 0$.)

Saffman (1987) (ii) Pure rotation (Mansour *et al.* 1991, $Ro = 0.247$, their Fig. 2(a)) (iii) Pure shear (Rogers *et al.* 1986, Case C128U).

3. Simulations and results

3.1 Initial conditions

The initial conditions for the simulations were obtained in the same way as those of Mansour *et al.* (1991). An initial energy spectrum was specified of the form

$$E(\kappa) = \kappa^4 \exp(-2(\kappa/\kappa_p)^2) \quad , \tag{4}$$

where κ_p is the location of the peak in the spectrum. For the runs described here κ_p was chosen to be either 24 or 48 depending on whether the number of grid points was nominally 128^3 or 256^3 respectively. The larger number of grid points and the larger κ_p means that those simulations have a larger computational domain size relative to the integral scales of the turbulence. The flow field was then evolved as decaying isotropic turbulence until it became fully developed as measured by the velocity derivative skewness obtaining a steady value near -0.5 and the turbulent kinetic energy displaying algebraic decay with a nearly constant decay rate. In practice it was found that by starting the simulations with a turbulent Reynolds number (see definition below) $Re_T = 823$ and allowing them to decay to $Re_T = 51$, the above conditions were met. This developed flow field was then used as initial conditions for the elliptic flow runs.

The simulations of Blaisdell & Shariff (1994) and those presented here do not match the Reynolds number of Mansour *et al.* We attempted to do so, but were confronted with the difficulty that, with the elliptic streamline flow, the large scales gain energy and quickly outgrow the computational domain. This problem does not occur for the pure rotation case where the turbulence simply decays. As a result, we found it necessary to change our initial conditions to make the computational domain larger relative to the initial integral scales of the turbulence. Because of the corresponding loss of resolution in the small scales, we reduced the Reynolds number.

The turbulent Reynolds number grows exponentially in the elliptic streamline flow and reaches values well over $1,000$ in the current DNS. However, because this is not an equilibrium flow, the turbulent Reynolds number is not a good indicator of the ratio of length scales in the problem or the degree of nonlinearity. As is shown below, it is found that the current DNS are affected by the low Reynolds numbers of the simulations. This means that the DNS data cannot be used in a quantitative way to test high Reynolds number turbulence models. However, a qualitative comparison is made below with two standard Reynolds stress models, which shows the models fail to predict the correct behavior, especially at larger rotation rates. In Section 4, suggestions are made for changing the method of generating the initial conditions so that the initial turbulent Reynolds number will not be so low. Higher Reynolds number simulations will allow quantitative comparison with Reynolds stress models and will provide more useful information.

3.2 Parameter space & linear theory

The governing nondimensional parameters for the elliptic streamline flow are (1) the aspect ratio of the elliptic streamlines, E, which is related to the ratio of the mean strain rate to the mean rotation rate, (2) the ratio of the turbulent time scale to a mean flow time scale, which can be measured either in terms of the mean flow strain as $S_e^* = ek/\varepsilon$ or in terms of the mean flow rotation as $S_\gamma^* = \gamma k/\varepsilon$, where k is the turbulent kinetic energy and ε is its dissipation rate, and (3) the turbulent Reynolds number, $Re_T = q^4/(\varepsilon\nu) = 4k^2/(\varepsilon\nu)$. The parameters used in the current simulations are shown in Table 1. Simulations e1-e5 are elliptic streamline flows with aspect ratios varying from 1.1 to 3.0. Simulations s1 and s1a are shear flow simulations and, therefore, have a value $E = \infty$. Most of the simulations are done with the same initial nondimensional strain rate. This was done in order to examine the effect of varying the mean flow rotation rate. This can be seen in Fig. 2 which shows the parameter space in terms of S_e^* and S_γ^*. The radial lines indicate a given aspect ratio, going from the 45° line for shear flow ($E = \infty$) to elliptic flows with $E = 3.0$, 2.0, 1.5, 1.25, and 1.1. Simulation e1 with $E = 1.1$ is off the scale of the plot. The circles give the initial values for each simulation and a given simulation is constrained to lie along one of the radial lines with a fixed aspect ratio, E. The values of S_e^* and S_γ^* will change as the turbulence develops, and it is believed that asymptotic values of these quantities should be approached. Simulation e2a has the same aspect ratio as e2, but the value of nondimensional strain rate is changed so that the nondimensional rotation rate is the same as that of the corresponding shear flow simulation, s1. The two shear flow simulations, s1 and s1a, differ in the initial Reynolds number.

It is helpful in interpreting the results of the current simulations to examine the predictions of linear stability theory within the parameter space shown in Fig. 2. A linear stability code employing the method of Landman & Saffman (1987) was used to compute the maximum inviscid growth rate as a function of strain rate, e, and rotation rate, γ. Fig. 3(a) shows a contour plot of the inviscid growth rate, σ. The nondimensional growth rate, σ/γ can be collapsed onto a single curve as shown by Landman & Saffman and given in Fig. 3(b). This curve corresponds to

Table 1. Initial condition and run parameters for the simulations.

Case	E	$S_{\gamma_0}^{\star}$	$S_{e_0}^{\star}$	Re_{T_0}	GRID	κ_p
e1	1.1	17.7527	1.68691	51	$128 \times 220 \times 128$	24
e2	1.25	7.68481	1.68691	51	$256 \times 440 \times 256$	48
e2a	1.25	1.68691	0.370297	51	$128 \times 220 \times 128$	24
e3	1.5	4.38597	1.68691	51	$256 \times 440 \times 256$	48
e4	2.0	2.81152	1.68691	51	$256 \times 440 \times 256$	48
e5	3.0	2.10864	1.68691	51	$256 \times 512 \times 256$	48
s1	∞	1.68691	1.68691	51	$128 \times 220 \times 128$	24
s1a	∞	1.68691	1.68691	102	$192 \times 330 \times 192$	24

a cross-section through the contour plot of Fig. 3(a) for a fixed rotation rate, γ, as indicated by the horizontal dotted line in Fig. 3(a). If the growth rate is nondimensionalized by the strain rate, one obtains the plot of σ/e shown in Fig. 3(c). This curve correspond to a cross-section through the contour plot of Fig. 3(a) for fixed strain rate, e, as indicated by the vertical dotted line. Bayly plotted the nondimensional growth rate as σ/Ω, where $\Omega = \sqrt{\gamma^2 - e^2}$ is the angular rotation rate for a fluid element as it traverses an elliptic streamline. This curve corresponds to a cross-section through the contour plot at a fixed Ω or through the nondimensional parameter space of Fig. 2 at a fixed Rossby number, $Ro = k/(e\Omega)$. Landman & Saffman point out that the plot of Bayly does not give a good indication of the behavior of the growth rate as one approaches pure shear, $\beta = 1$. The most complete picture, however, comes from the contour plot in Fig. 3(a) together with the cross-sections in Figs. 3(b) and (c). For cases with a fixed initial rotation rate, there is an aspect ratio for which the growth rate is a maximum (near $E = 3.0$). For cases with a fixed initial strain rate, the growth rate increases as the rotation rate increases. For cases with a fixed initial Rossby number, the growth rate decreases as the rotation rate increases. Therefore, the effect of rotation cannot be put into the simple statement that strong rotation suppresses the growth of turbulence, as is often assumed. In the sections that follow, the growth rate of the turbulence within the DNS will be examined and the trends will be compared to those seen from the linear theory.

3.3 Turbulence evolution

The elliptic streamline flow is linearly unstable for any non-zero strain rate, e. From the linear theory the turbulent kinetic energy grows exponentially. Larger length scales are not affected by viscosity and have a larger growth rate. Therefore, eventually the flow becomes dominated by larger and larger length scales. When this happens the energy containing eddies outgrow the computational domain. They
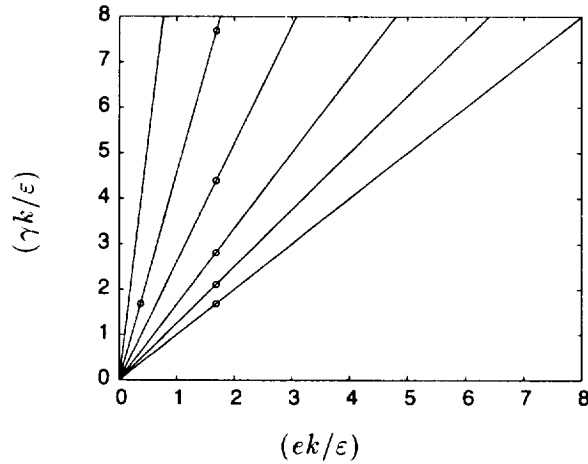
FIGURE 2. Parameter space based on the initial nondimensional strain rate and rotation rate. The 45° line corresponds to shear flow ($E = \infty$). The other radial lines are for $E = 3.0$, 2.0, 1.5, 1.25 and 1.1. The circles indicate the initial conditions for the current simulations.

become affected by the periodic boundary conditions and the statistics are no longer reliable.

Since the dominant effect of rotation on the turbulence is to suppress the nonlinear cascade, it is useful to have a measure of the nonlinear transfer of energy from large scales to small scales. Mansour *et al.* (1991) used a generalized skewness defined by

$$S = -\frac{6\sqrt{15}}{7}\frac{\int \kappa^2 T(\kappa)\,d\kappa}{\left(\int \kappa^2 E(\kappa)\,d\kappa\right)^{3/2}} \quad , \tag{5}$$

where κ is the magnitude of the wavenumber vector, $E(\kappa)$ is the three-dimensional energy spectrum, $T(\kappa)$ is the transfer spectrum, and the numerical prefactor is such that for isotropic turbulence S is approximately -0.5.

The evolution of the skewness S is shown in Fig. 4(a) for simulations which span the range of aspect ratios $E = 1.25$, 1.5, 2.0, and 3.0. As soon as the mean flow is turned on, the skewness begins to drop in magnitude, indicating that the nonlinear cascade is inhibited. The cases with lower aspect ratios (more dominated by rotation) have a skewness that comes closer to zero. So, as one would expect, stronger rotation leads to stronger suppression of the nonlinear processes. Interestingly enough the simulations show that the skewness recovers at later times as the turbulence grows. Also, it seems that the skewness approaches an asymptotic value that is the same for all aspect ratios, although the case with $E = 1.25$ could not be carried far enough in time to see if the skewness recovers fully.

The linear stability analysis of the elliptic streamline flow indicates that the turbulent kinetic energy grows exponentially. A nondimensional growth rate can be defined by
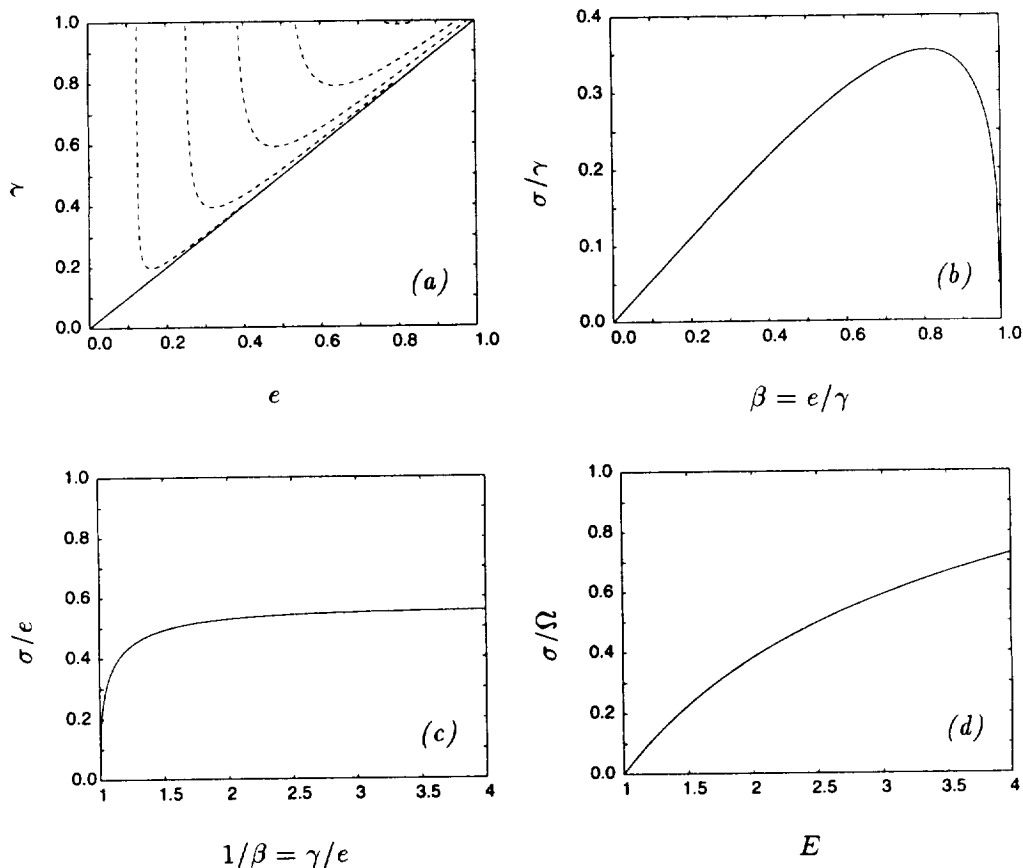
$$\frac{1}{ek}\frac{dk}{dt} \quad . \tag{6}$$

FIGURE 3. *(a)* Contours of inviscid growth rate σ. *(b)* Nondimensional growth rate for constant γ. *(c)* Nondimensional growth rate for constant e. *(d)* Nondimensional growth rate for constant Ω.

This nondimensional growth rate is shown in Fig. 4(b) for the same series of simulations as above. After the flow develops for a while a roughly constant positive level is reached, which indicates that k is growing exponentially. The growth rate nondimensionalized by the strain rate, e, is highest for the case with the lowest aspect ratio (strongest rotation), which is in agreement with the trend of the linear stability analysis shown in Fig. 3(c). However, at later times the simulations seem to change to a lower growth rate as nonlinear effects become more important. Without carrying the simulations further in time it is difficult to determine whether they approach a universal growth rate that is independent of aspect ratio.

One concern about the current simulations is that the initial Reynolds number is very low. In order to use the DNS results for comparisons with high Reynolds number formulations of turbulence models, the nondimensional turbulent statistics should be independent of Reynolds number. For the current simulations that is not the case. Figs. 5(a) and (b) show the skewness and the growth rate for the two shear
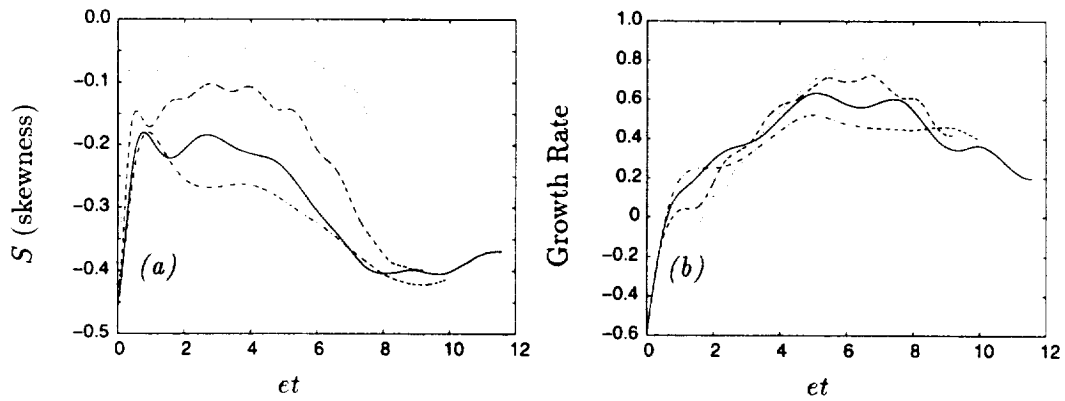
FIGURE 4. (a) Generalized skewness and (b) nondimensional growth rate of the turbulent kinetic energy for cases e2 (········), e3 (----), e4 (———), and e5 (—·—).
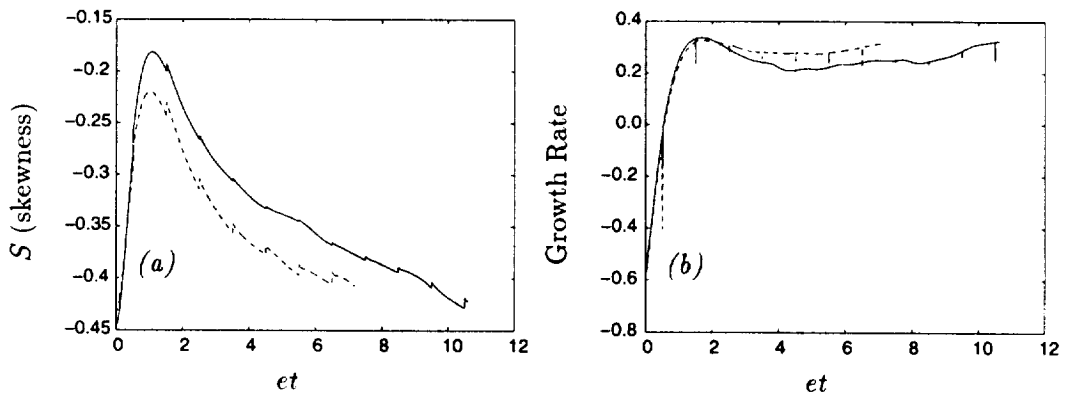

FIGURE 5. (a) Generalized skewness and (b) nondimensional growth rate of the turbulent kinetic energy for cases s1 (———), s1a (----).

flow simulations s1 and s1a. Simulation s1 is similar to the elliptic streamline flow simulations that are described above. Simulation s1a has a higher initial turbulent Reynolds number, as shown in Table 1. The larger grid for case s1a is in order to ensure adequate resolution of the small scales. As shown in Fig. 5 there is a significant difference in the skewness and the growth rate for the two runs, which can be attributed to the differences in Reynolds number. The sudden jumps are an artifact of the periodic remeshing process used in the shear flow simulations (see Rogallo 1981). The low Reynolds numbers of the current simulations is caused by having a long period of isotropic decay before the elliptic flow runs are begun. Alternate methods that would allow the initial Reynolds number to be much higher are discussed in section 4.

Most of the simulations in this study have the same initial strain rate. This was done in order to focus on the effect of mean flow rotation. In order to make the study more complete, simulations were also done with a fixed initial mean rotation
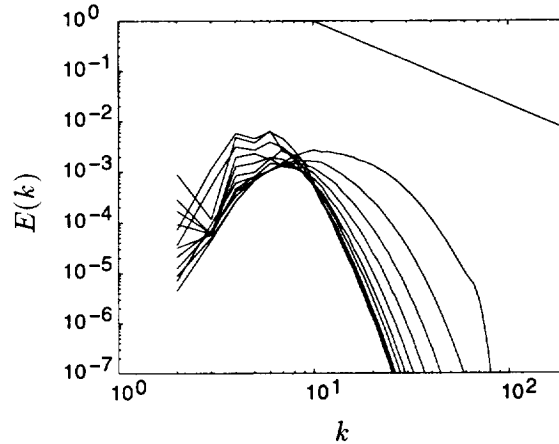
FIGURE 6. Development of the three-dimensional energy spectrum, $E(k)$, for case e2a.

rate, such as cases e2a and s1. However, cases with low aspect ratios and low mean rotation rates are difficult to do. The problem can be seen in Fig. 6, which shows the evolution of the three-dimensional energy spectrum for elliptic flow e2a. The energy in the small scales continually decays while energy in the large scales grows from the instability. The large scales quickly outgrow the computational box as indicated by the spectrum at low wavenumbers. It seems that it would be desirable to simply reduce the resolution of the small scales and increase the computational domain size. However, this cannot be done without compromising the resolution of the isotropic initial conditions. A simple analysis can be done to explain the behavior seen in Fig. 6. From the viscous analysis of Landman & Saffman, there is a high wavenumber cut-off beyond which the flow is stable. This wavenumber is given by a critical Ekman number, $E_\gamma(\beta) = 2\pi\nu\kappa_0^2/\gamma$, where κ_0 is the magnitude of the critical wavenumber. Using $Re_T = q^4/(\varepsilon\nu)$ and $S_\gamma^* = \gamma k/\varepsilon$, the definition of the critical Ekman number can be rearranged to give

$$\frac{\kappa_0}{\kappa_p} = \left(\frac{\varepsilon}{\kappa_p q^3}\right)\left[\frac{E_\gamma(\beta)Re_T S_\gamma^*}{\pi}\right]^{1/2} \quad , \tag{7}$$

where κ_p is the peak in the instantaneous energy spectrum. Taking a value of $\varepsilon/(\kappa_p q^3) = 0.28$, $\beta = 0.22$, and $E_\gamma(\beta) = 0.6$ gives, $\kappa_0/\kappa_p = 1.1$. Therefore, for simulation e2a the viscous cut-off wavenumber is at about the peak in the energy spectrum from the decayed isotropic initial conditions, which seems to correspond roughly to what is observed in Fig. 6.

It is desirable to have a greater fraction of the wavenumbers used in the simulation in the unstable range. In order to perform good quality simulations one needs κ_0/κ_p to be large (preferably at least 2). Equation (7) shows that this is more difficult for simulations with lower nondimensional rotation rates, S_γ^*, and that to achieve this, simulations with higher Reynolds numbers are needed.
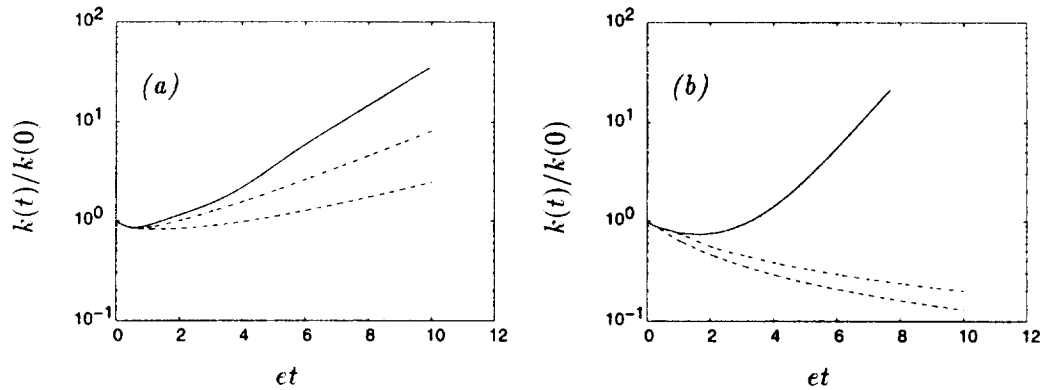
FIGURE 7. Nondimensional turbulent kinetic energy, k, from the DNS (———), using the LLR model (—·—), and using the SSG model (----) for *(a)* case e5 with $E = 3.0$ and *(b)* case e2 with $E = 1.25$.

3.4 Comparison with turbulence models

A brief comparison is made between the DNS data for the elliptic streamline flow and two standard Reynolds stress models — the Launder, Reece and Rodi (1975) model (LRR) and the Speziale, Sarkar and Gatski (1991) model (SSG). It must, however, be borne in mind that the comparison being made is between low Reynolds number DNS data and high Reynolds number formulations of the turbulence models. Figs. 7(a) and (b) show the comparison for the nondimensional turbulent kinetic energy for cases e5 and e2 with $E = 3.0$ and 1.25 respectively. For the case with $E = 3.0$, which is not so dominated by strong rotation, the models predict exponential growth. However, the growth rate is substantially lower than that seen in the DNS. The LLR model gives a higher growth rate than the SSG model because the SSG model is sensitized to rotation and reduces the growth rate for strong rotation. Based on the growth rates seen at later times in Fig. 4(b), DNS at higher Reynolds numbers may give lower growth rates, which would be closer to those of the models.

In Fig. 7(b) the comparison is made for the case with $E = 1.25$, which is more rotation dominated. For this case both models predict decay while the DNS shows exponential growth. Here the models are seen to give the wrong qualitative behavior. Speziale *et al.* (1996) have pointed out the need for turbulence models to predict growth for flows that are linearly unstable. Clearly standard Reynolds stress models fail for strongly rotating flows, and there is a need for model improvement.

4. Conclusions and suggestions for future work

The study of the elliptic streamline flow begun by Blaisdell & Shariff (1994) has been continued by performing simulations over a range of parameters. The elliptic streamline flow is a homogeneous turbulent flow that combines solid body rotation and strain. It is an important flow for understanding the effects of rotation on engineering turbulent flows.

For short times the imposition of the mean flow suppresses the nonlinear cascade, but at later times nonlinearity is reestablished. As evidenced by the skewness, the growth rate of the turbulent kinetic energy, and other statistics, the turbulence seems to develop toward an asymptotic state that is independent of the ratio of mean rotation to mean strain.

A comparison with standard Reynolds stress models shows that the models fail to give the correct qualitative behavior for large rotation rates. However, the current simulations have a very low initial turbulent Reynolds number and, therefore, meaningful quantitative comparisons with the models cannot be made.

Future simulations should be done at higher Reynolds numbers. One reason for the low Reynolds numbers of the current simulations is the method of generating initial conditions. The initial conditions for the elliptic flow simulations are taken from fully developed decaying isotropic turbulence. During the isotropic decay the Reynolds number falls to very low values. One approach to overcome this is to not have any isotropic decay period, similar to the shear flow simulations of Rogers *et al.* (1986). The mean flow would be turned on with randomly generated initial conditions. A disadvantage of this method is that turbulence models cannot be expected to follow the unphysical development at early time; however, comparisons can be made with turbulence models by starting the initial conditions for the model calculations using the DNS data at some time after the flow has developed. A second method to produce higher Reynolds number isotropic initial conditions is to artificially keep the turbulent Reynolds number fixed at a high value by changing the viscosity before allowing the turbulence to decay. This was done by Blaisdell *et al.* (1991) and produces developed isotropic turbulence at a relatively high Reynolds number. Both approaches are being pursued.

Acknowledgements

REFERENCES

BAYLY, B. J. 1986 Three dimensional instability of elliptic flow. *Phys. Rev. Lett.* **57**, 2160–2171.

BENOIT, J.-P. 1992 Etude expérimentale et théorique d'une turbulence homogéne soumise à des effets couplés de rotation et de déformation plane. Ph.D. thesis, L'Ecole Central de Lyon, France.

BLAISDELL, G. A., MANSOUR, N. N. & REYNOLDS, W. C. 1991 Numerical simulation of compressible homogeneous turbulence. Thermosciences Division Report TF-50, Stanford University, Stanford, California.

CAMBON, C., BENOIT, J. P., SHAO, L. & JACQUIN, L. 1994 Stability analysis and large-eddy simulation of rotating turbulence with organized eddies. *J. Fluid Mech.* **278**, 175.

CAMBON, C., TEISSÈDRE, C. & JEANDEL, D. 1985 Etude d'éffets couplés de déformation et de rotation sur une turbulence homogéne. *J. Méc. Théo. Appl.* **4**, 629.

LANDMAN, M. J. & SAFFMAN, P. G. 1987 The 3-D instability of strained vortices in a viscous fluid. *Phys. Fluids.* **30**, 2339–2342.

LAUNDER, B. E., REECE, G. & RODI, W. 1975 Progress in the development of a Reynolds stress turbulence closure. *J. Fluid Mech.* **68**, 537.

LUNDGREN, T. S. & MANSOUR, N. N. 1996 Transition to turbulence in an elliptic vortex. *J. Fluid Mech.* **307**, 43–62.

MALKUS, W. V. R. 1989 An experimental study of global instabilities due to the tidal (elliptical) distortion of a rotating elastic cylinder. *Geophys. Astrophys. Fluid Dyn.* **48**, 123–134.

MALKUS, W. V. & BERRY, M. E. 1988 Order and disorder in planetary dynamos. *Summer Study Program in Geophysical Fluid Dynamics*, (eds. W. V. Malkus and M. E. Berry).

MANSOUR, N. N., CAMBON, C. & SPEZIALE, C. G. 1991 Single point modeling of initially isotropic turbulence under uniform rotation. Center for Turbulence Research, *Annual Research Briefs*, NASA Ames/Stanford Univ.

PIERREHUMBERT, R. T. 1986 Universal short-wave instability of two-dimensional eddies in an inviscid fluid. *Phys. Rev. Lett.* **57**, No. 17, 2157–2159.

ROGALLO, R. S. 1981 Numerical experiments in homogeneous turbulence. NASA Technical Memorandum 81315.

ROGERS, M. M., MOIN, P. & REYNOLDS, W. C. 1986 The structure and modeling of the hydrodynamic and passive scalar fields in homogeneous turbulent shear flow. Thermosciences Division Report TF-25, Stanford University, Stanford, California.

SPEZIALE, C. G., ABID, R. & BLAISDELL, G. A. 1996 On the consistency of Reynolds stress turbulence closures with hydrodynamic stability theory. *Physics Fluids.* **8**, 781–788.

SPEZIALE, C. G., SARKAR, S. & GATSKI T. B. Modeling the pressure-strain correlation of turbulence: An invariant dynamical systems approach J. Fluid Mech. *227.* **245.**

WALEFFE, F. 1990 The three-dimensional instability of strained vortices. *Phys. Fluids A.* **2**, 76–80.

WIDNALL, S. E., BLISS, D. B., & TSAI, C.-Y. 1974 The instability of short waves on a vortex ring. *J. Fluid Mech.* **66**, 35–47.